Imaging nuclear spins weakly coupled to a probe paramagnetic center

Abdelghani Laraoui, Daniela Pagliero, and Carlos A. Meriles

Phys. Rev. B **91**, 205410 — Published 11 May 2015

DOI: 10.1103/PhysRevB.91.205410

Imaging nuclear spins weakly coupled to a probe paramagnetic center

Abdelghani Laraoui[1], *Daniela Pagliero*[1], *Carlos A. Meriles*[1]

[1]Dept. of Physics, CUNY-City College of New York, New York, NY 10031, USA.

Abstract

Optically-detected paramagnetic centers in wide-bandgap semiconductors are emerging as a promising platform for nanoscale metrology at room temperature. Of particular interest are applications where the center is used as a probe to interrogate other spins that cannot be observed directly. Using the nitrogen-vacancy center in diamond as a model system, we propose a strategy to determining the spatial coordinates of weakly coupled nuclear spins. The central idea is to label the target nucleus with a spin polarization that depends on its spatial location, which is subsequently revealed by making this polarization flow back to the NV for readout. Using extensive analytical and numerical modeling, we show that the technique can attain high spatial resolution depending on the NV lifetime and target spin location. No external magnetic field gradient is required, which circumvents complications resulting from changes in the direction of the applied magnetic field, and considerably simplifies the required instrumentation. Extensions of the present technique may be adapted to pinpoint the locations of other paramagnetic centers in the NV vicinity or to yield information on dynamical processes in molecules on the diamond surface.

Nuclear magnetic resonance (NMR) excels in its ability to probe non-destructively the structure and dynamics of molecular moieties without the need for long-range order, but the low detection sensitivity inherent to inductive detection limits this technique to ensemble measurements. Magnetic resonance force microscopy (MRFM) was introduced two decades ago precisely to circumvent this problem[1]. The idea was to leverage on the extreme sensitivity and magnetic field gradients of MRFM probes to discriminate between signals from individual nuclear sites in a molecule so as to image its structure with atomic resolution. Despite enormous progress[2], however, this latter goal has proven exceedingly difficult, mainly due to the minute ratio between the spin and thermal energies, even at the lowest temperatures possible today.

A more recent route to nanoscale magnetic resonance builds on the properties of select paramagnetic centers in solid-state matrices. At the core of this form of sensing is a singular combination of transition rules and decay rates between electronic states, responsible for the up-conversion of spin-flip-induced energy differences into, e.g., changes in the center's fluorescence. Case systems presently under intense study are the di-vacancy and silicon-vacancy centers in SiC[3-5], rare-earth ions in garnets[6,7], substitutional phosphorous[8] and bismuth[9] in silicon, and the nitrogen-vacancy (NV) center in diamond[10]. Common to these systems is the ability to individually initialize, manipulate, and readout the paramagnetic center spin via a combination of microwave (mw) and optical (or electrical) pulses, often under ambient conditions. These unique features are being presently exploited to probe other spins in the paramagnetic center vicinity that cannot be directly initialized or interrogated. For example, nitrogen-vacancy (NV) centers engineered near the diamond surface have been used to detect small ensembles of protons from organic films or fluids in contact with the crystal surface[11,12]. Subsequent experiments[13] have demonstrated the detection of other spin species including ^{19}F,

and ^{31}P, with more recent studies reporting the observation of individual ^{1}H and ^{29}Si spins[14,15]. In this light, schemes designed to determine the spatial location of individual nuclear (or electronic) spins with atomic resolution gain particular interest as they are likely to become a key ingredient in, e.g., the characterization of the structure and dynamics of individual molecules adsorbed onto the center's solid-state host.

Here we introduce an imaging protocol that builds on the hyperfine-induced gradient to selectively mediate the transfer and retrieval of spin polarization between the paramagnetic center and neighboring nuclei. In many ways, our approach follows the principles of radar technology where a probe 'signal'—in the form of spin polarization—scouts the vicinity in search for a 'target'. In our scheme, the location of the target—i.e., a nuclear spin—is determined as the 'reflected' polarization travels back to the source. The target's spatial coordinates are reconstructed from the angle where the reflection took place and the round trip time, here encoded in the pulse phases and duration of our magnetic resonance sequence. Both the range and spatial resolution depend on the coherence lifetime of the paramagnetic center, which varies from one spin system to another. For concreteness, we consider the particular case of an NV center interacting with distant (i.e., 0.5 nm or more) nuclear spins. We find that the spatial resolution—itself a complex function of the nuclear spin location and NV lifetimes—is sufficient to image small NV/^{13}C clusters without the need for external magnetic field gradients and is limited by the NV spin coherence lifetime. Since the applied magnetic field remains unchanged, our approach circumvents complications arising from NV level mixing and can be extended to high field (where changing the relative sample orientation is often impractical). Therefore, these ideas complement recent experimental work where the coordinates of individual proton spins

from molecules on the diamond surface are determined by systematically altering the field direction in the presence of dynamical decoupling[14].

To more formally introduce our imaging scheme, we start by considering the individual NV-^{13}C spin pair highlighted in Fig. 1a. Here we take a reference frame centered at the NV—a system with spin number $S = 1$—and use the spherical coordinates (r, θ, φ) to indicate the location of the ^{13}C nucleus—featuring a spin number $I = 1/2$. We assume that the NV and z-axis are parallel and co-linear with an externally applied magnetic field B_0. The system Hamiltonian is then given by

$$H = \Delta S_z^2 - \gamma_S B_0 S_z - \gamma_I B_0 I_z + A_{z\parallel} S_z I_z + A_{z\perp} S_z I_\varphi \,, \qquad (1)$$

where, as usual, we have truncated non-secular contributions, $\Delta = 2\pi \times 2.87$ GHz denotes the NV zero-field splitting, γ_S (γ_I) is the NV (^{13}C) gyromagnetic ratio, S_z and I_z are the z-projections of the NV and ^{13}C spin operators, and $I_\varphi \equiv I_x \cos\varphi + I_y \sin\varphi$, with φ denoting the nuclear spin azimuthal angle (Fig. 1a). For a distant carbon, the NV-^{13}C coupling is dipolar in nature and the hyperfine constants take the form $A_{z\parallel} = k\,(3cos^2\theta - 1)/r^3$ and $A_{z\perp} = 3k\,cos\theta\,sin\theta/r^3$ where $k \equiv \mu_0 \gamma_{NV} \gamma_C \hbar/(4\pi)$, μ_0 is the vacuum permeability, and $\hbar$ is Planck's constant divided by 2π. In a typical magnetic resonance experiment, microwave (mw) pulses induce transitions between two selected states of the NV ground state triplet thus rendering the NV a two-level system with characteristic frequency ω_S. The system evolution can thus be described via the simplified Hamiltonian

$$H^* = A_{z\parallel} S_z I_z + A_{z\perp} S_z e^{-i\omega_I t I_z} I_\varphi e^{i\omega_I t I_z} \,, \qquad (2)$$

where the star denotes a transformation to the doubly rotating frame at the NV and ^{13}C Larmor frequencies, and we have ignored rapidly fluctuating terms (see Section S1 of the Supplementary Material). Unless otherwise noted, we will assume that the hyperfine coupling is weak compared

to the nuclear Zeeman field, i.e., $A_{z\parallel}, A_{z\perp} \ll \omega_I \equiv \gamma_I B_0$. Note that the comparatively strong hyperfine coupling with the nitrogen host can be ignored, because the nitrogen nuclear spin does not significantly evolve during the typical time interval of an NV protocol (~1 ms or less). Further, the nitrogen nuclear spin can be initialized if so required, as demonstrated recently[16] (see also Section S1 in the Supplementary Material).

To scout for nuclear spin targets we make use of the INEPT-like[17] polarization transfer protocol in Fig. 1b comprising a train of mw pulses on the NV spin (a 'CPMG train') followed by an interval of free evolution and a radio-frequency pulse resonant with the ^{13}C frequency (see below). For reasons that will be apparent shortly, we assume that all mw pulses induce transitions between the $m_S = \pm 1$ states, possible via the use of composite pulses[18] or multi-frequency excitation[19]. Throughout the protocol, both the duration of the train and the free evolution interval—respectively denoted as t_1, t_2—are systematically increased; in the case of t_1, the increments are in units of τ—coincident with half the ^{13}C Larmor period—and accompanied by the addition of a new π-pulse at each step. To best appreciate the combined effect of the pulse sequence we first note that over a unit $\tau/2$—π—τ—π—$\tau/2$ of the CPMG train the effective system evolution can be calculated from the average Hamiltonian[20]

$$H_1^* \approx \int_0^{\tau/2} H^*(t)\,dt - \int_{\tau/2}^{3\tau/2} H^*(t)\,dt + \int_{3\tau/2}^{2\tau} H^*(t)\,dt = \frac{2}{\pi} A_{z\perp} S_z I_\varphi \ . \qquad (3)$$

independent of $A_{z\parallel}$ (see Section S1 of the Supplementary Material). The alternating sign in the sum above results from the cumulative effect of the π-pulses, here inverting the populations between the $m_S = \pm 1$ states and consequently mapping S_z into $-S_z$ each time. Conversely, the effective Hamiltonian governing the t_2 interval is given by

$$H_2^* \approx \int_0^{t_2} H^*(t)\,dt = A_{z\parallel} S_z I_z \ , \qquad (4)$$

independent of $A_{z\perp}$. Note that the stronger interaction of the NV spin with the host nitrogen nucleus can be ignored altogether when microwave pulses are sufficiently broadband (the typical condition in practice); alternatively this interaction can be effectively cancelled by conveniently prepolarizing the ^{14}N spin (see Section S1 of the Supplementary Material).

We now calculate the system evolution, which, for simplicity, we restrict to the case where t_1 and t_2 take the (optimum) values $t_1^{opt} \equiv \pi^2/(4A_{z\perp})$, and $t_2^{opt} = \pi/(2A_{z\parallel})$ (see Section S2 of the Supplementary Material for a full derivation). Starting from a state where the NV is in $m_S = +1$ and the nuclear spin is unpolarized, the system density matrix $\rho(t)$ before and after application of the CPMG train takes the form

$$\rho(t=0) = \frac{1}{4}(1 - P_0 + S_z) \rightarrow \rho\left(t_1^{opt}\right) = \frac{1}{4}\left(1 - P_0 + 2\alpha S_z I_\varphi\right) , \qquad (5)$$

where P_0 denotes the projection operator into $m_S = 0$ and $\alpha \equiv sgn(A_{z\perp})$. The last term in the expression for $\rho\left(t_1^{opt}\right)$ corresponds to an antiphase nuclear spin coherence, i.e., a nuclear spin precession whose sign is conditioned on the orientation of the NV polarization. Importantly, the phase φ of this coherence depends on the nuclear spin azimuthal coordinate, which, as we show below, will help us pinpoint the ^{13}C location. To complete the polarization transfer, the system is allowed to evolve for a time t_2^{opt} before applying an rf π/2-pulse. For the simpler case where $\phi = \varphi + m\pi$ with m integer, the net result is the transformation

$$\rho\left(t_1^{opt}\right) \rightarrow \rho\left(t_2^{opt}\right) = \frac{1}{4}(1 - P_0)(1 + 2\delta I_z) , \qquad (6)$$

where we define $\delta \equiv sgn\left(A_{z\parallel}A_{z\perp}cos(\varphi - \phi)\right)$. The expression for $\rho\left(t_2^{opt}\right)$ corresponds to a state where the NV is equally likely to point up or down (i.e., a depolarized state in the $m_S = \pm 1$ subspace) and the nuclear spin is polarized to $m_I = +1/2$ or $m_I = -1/2$ depending on the sign of δ.

A numerical calculation of the nuclear spin response for an arbitrary number of pulses or duration of the free evolution interval is presented in Fig. 2a for the particular case of a $^{!3}$C spin in a ~30 mT field ($\omega_I/2\pi = 320$ kHz) with spatial coordinates $r = 0.9$ nm, $\theta = 70.5°$, and $\varphi = 0$ (corresponding to $A_{z\perp}/2\pi = 26$ kHz and $A_{z\parallel}/2\pi = -19$ kHz). Complete nuclear spin polarization of alternating sign is only attained at multiples of t_1^{opt} and t_2^{opt}, each of which reacts independently to a change of $A_{z\perp}$ or $A_{z\parallel}$ (see right panels in Fig. 2a). The latter is more clearly shown in Fig. 2b where we plot the calculated temporal coordinates of the first peak transfer (in this example resulting in negative nuclear spin polarization) as we systematically vary either dipolar coupling constant. The analytical model agrees well with the numerical calculation in the (valid) regime where the nuclear Larmor frequency is sufficiently large (at least five times greater than the coupling). We also confirm the $2/\pi$ scaling of $A_{z\perp}$ anticipated in Eq. (3) using average Hamiltonian theory.

While in the calculations above mw pulses selectively act on the $m_S = \pm 1$ states, it is also possible to induce full nuclear polarization using a single quantum NV transition (i.e., $m_S = 0 \leftrightarrow m_S = \pm 1$), as we numerically demonstrate in Fig. 2c. However, rather than oscillating between states of positive and negative polarization, the nuclear spin polarizes or not depending on the chosen timing. Optimal transfer times comparable to those in Fig. 2a can be attained by increasing the dipolar coupling constants indicating that the down-scaling noted above is more pronounced for a single quantum transition. Further, both t_1^{opt} and t_2^{opt} are influenced by a change in either coupling constants (central and right panels in Fig. 2c) pointing to a more complicated relationship between the sequence timing and the strength of the dipolar interaction. The latter can be understood by noting that a single-quantum π-pulse is insufficient

to change the sign of S_z meaning that contributions of the form AS_zI_z in Eq. (2) are not averaged out during the CPMG train.

We noted above that the nuclear/electron antiphase coherence generated by the CPMG train depends on the nuclear spin azimuthal angle φ (see Eq. (5)). The latter has a direct impact on the resulting nuclear polarization, shown in Fig. 3a as we rotate the carbon location about the z-axis: For given evolution intervals t_1, t_2, the nuclear polarization exhibits a sinusoidal dependence on φ whose amplitude ranges from the maximum possible (e.g., at the first peak transfer, red curve) to zero (e.g., at a nodal point, black curve). We interpret this behavior as a manifestation of the broken axial symmetry in the system Hamiltonian (Eqs. (1) and (2)), which, in turn, stems from the large difference between the electron and nuclear resonance frequencies. Fast manipulation of the paramagnetic center synchronic with ω_I during the CPMG train creates a resonant time-dependent field at the nuclear site, which leads to the appearance of nuclear spin (anti-phase) coherence. Since this field depends on the carbon azimuthal angle, it imprints the resulting nuclear spin coherence with a φ-dependent phase. Consequently, conversion to nuclear polarization requires control of ϕ—the rf phase *in the laboratory frame*—easily attained in practice, e.g., by direct rf pulse synthesis. As we show below, this ability will prove key to identifying the spatial location of the nuclear spin.

Besides the rf phase, the interpulse separation in the CPMG train is another parameter worth commenting on. For the NV-^{13}C geometry considered above, Fig. 3b shows the dependence of the nuclear polarization P_I on τ and t_2 for CPMG trains with different number n of π-pulses. For $\omega_I\tau/2\pi = 0.5$ and $\phi = 0$ (left panels), we find that the transfer efficiency is optimum at $n = 10$ and vanishes as $n \to 20$, in agreement with the results of Fig. 2a. However, nuclear polarization does build up as τ departs from half the ^{13}C Larmor period. This effect is

more pronounced for larger values of n indicating that spin transfer to more weakly coupled nuclei is increasingly susceptible to imperfections in the timing of the CPMG train. This tendency is replicated in the case $\phi = 90$ (right panels), where the spin transfer is prevented only if τ precisely coincides with π/ω_I.

To determine the nuclear spin coordinates we use a composite sequence where the protocol in Fig. 1 — designed to transfer spin polarization from the electron spin *S* to the nuclear spin *I* — is followed by NV re-initialization and nuclear spin polarization retrieval. The latter can be implemented in various ways, for example, by running the transfer protocol in reverse (Fig. 4a, see also Fig. S1 of the Supporting Material). By systematically increasing the polarization exchange intervals t_1 and t_2 and the rf phase ϕ one gathers a 3D data set that reflects on the efficiency of the transfer and hence on the coordinates of the target nuclear spin (Fig. 4b). Fourier transforming along t_1 and t_2 produces a set of extrema in the 3D space spanned by $A_{z\parallel}$, $A_{z\perp}$ and φ (Fig. 4c), which can then be converted into real-space coordinates. The result is presented in Fig 4d for the example case of Figs. 2 and 3 (single spin with coordinates ($r = 0.9$ nm, $\theta = 70.5°$, $\varphi = 0°$). Besides the 'real' nuclear site (dashed line in Fig. 4d), we identify an accompanying set of 'ghost' images, as expected in the case of a symmetric transfer/retrieval protocol (where the NV signal is insensitive to the absolute signs of $A_{z\parallel}$, $A_{z\perp}$ and ϕ, Section S2.2 of the Supplementary Material); two possible sites result from each sign ambiguity, thus leading to a total of eight possible locations. For future reference, we also note the crescent shape of the isolevel surfaces, and the correspondingly poor azimuthal resolution.

All ambiguities on the true location of the nuclear site can be removed by breaking the symmetry between the transfer and retrieval segments of the protocol—a mirror image of each other in Fig. 4. For illustration purposes, Fig. 5a introduces an alternate retrieval sequence where

the cyclic application of inversion pulses makes the effective Hamiltonian equal to $H_1^* = \frac{2}{\pi} A_{z\perp} S_z I_\varphi$ during both evolution intervals, $\tilde{t}_1$ and $\tilde{t}_2$. Unlike the result in Figs. 4c and 4d, it can be shown that the accompanying NV signal has an overall sign that depends on $\alpha \equiv sgn\{A_{z\perp}\}$, and $\beta \equiv sgn\{A_{z\parallel}\}$ but not on $\gamma \equiv sgn\{\cos(\phi - \phi)\}$. Other combinations are possible with complementary pulse protocols, which allows one to independently determine α, β, and γ (and correspondingly the 'true' nuclear site). The result is presented in Fig. 5b for the more complex case of multiple ^{13}C spins weakly coupled to an NV (Section S2 of the Supplementary Material).

An important practical consideration in the application of this technique is the limit spatial resolution, in general, a complex function of various parameters. The most relevant factor is the NV coherence lifetime T_{2NV}, of immediate impact on the duration of the NV response and thus on the broadening of the resulting 'peaks' in the 3D spectrum. An example is presented in Fig. 5c, where we compare the 'images' of the same ^{13}C cluster for three different NV lifetimes (150 μs, 75 μs, and 38 μs). In all cases we have ignored NV spin-lattice relaxation (>1 ms in moderately pure diamond) and broadening originating from nuclear spin decoherence or nuclear spin-lattice relaxation (with time scales of ~10 ms, and 1 s or greater, respectively). Shorter T_{2NV} selectively impact the radial and polar resolution while the azimuthal resolution remains unchanged (see below). In particular, for $T_{2NV} \sim 100$ μs and $A_{z\parallel}, A_{z\perp} \sim 30$ kHz, we find $\Delta r \sim 0.1$ nm and $\Delta\theta \sim 4$ deg. We warn, however, that these estimates serve only as a crude reference: For a fixed NV lifetime, the spatial resolution decreases as the hyperfine coupling weakens, simply because a longer interaction time is required to exchange polarization with the target nuclear spin. For example, additional calculations (not shown here for brevity) indicate that the volume enclosed by the isolevel surface in Fig. 5b quadruples when increasing the nuclear distance r by

a factor ~1.8, from 0.9 nm to 1.6 nm. Naturally, similar effects are observed as the polar angle approaches $\theta = 0^{\circ}$ or $\theta = 54.7^{\circ}$, respectively the nodes of $A_{z\perp}$ and $A_{z\parallel}$.

Further work will be needed to circumvent some present limitations, including the extended crescent shape—and correspondingly moderate resolution—along the azimuthal angle φ (Fig. 4d). This coordinate differs from the other two in that it is defined by the phase selectivity of the nuclear spin projection pulses throughout the polarization exchange ($P_S \propto \cos^2(\varphi - \phi)$, Section S2.2 of the Supplementary Material). Higher azimuthal selectivity may be attained, for instance, via the use of composite rf π/2-pulses more sensitive to the nuclear spin phase.

The ideas underlying the technique presented herein can be extended in several complementary directions. First, we emphasize that spins other than the NV can be envisioned as the source of nuclear spin polarization. Besides the various paramagnetic centers mentioned above, one possibility is the use of 'dark' electronic spins such as the P1 center in diamond (formed by a substitutional nitrogen), already shown to polarize by contact with the NV[21]. Alternatively, one can envision the use of paramagnetic labels (e.g., nitroxyls) to mediate the interaction between the NV and nuclear spins in outer molecules, as demonstrated recently[14]. Along these lines, we mention that our technique could be conceivably adapted to determine the spatial positions of electronic rather than nuclear spins. Such strategy would be helpful in pinpointing the positions of key sites within molecules tethered to the diamond surface[22]. Further, since the polarization transfer efficiency depends on the exact spatial coordinates of the target (electronic or nuclear) spin, introducing a variable time interval between polarization transfer and retrieval could be exploited to monitor various dynamical processes. Examples are slow molecular folding processes activated externally either by chemical or optical means.

Purely as a polarization transfer strategy, our approach could serve as a route to dynamically polarize organic systems adsorbed on the diamond surface[23]. In particular, because the pulse timing can be controlled with nanosecond precision (much shorter than the microsecond nuclear Larmor period at moderate magnetic fields), the time jitter is expected to be low, thus ensuring high spin transfer efficiency. The latter may prove an advantage when compared to, e.g., the Hartman-Hahn scheme[24], where amplitude fluctuations of the rf field reduce the probability of a flip-flop, especially for weakly coupled nuclei. The flipside, however, is the greater sensitivity to inter-nuclear spin interactions, which, in the present protocol, must remain smaller than the coupling to the NV. While this is typically the case within the diamond crystal (where ^{13}C spins are dilute), the opposite limit applies to nuclei on the diamond surface (such as ^{1}H spins in adsorbed molecules). This complication could be somewhat mitigated, e.g., via the combined use of inter-nuclear dynamical decoupling sequences.

The authors acknowledge support from the National Science Foundation.

References

[1] J.A. Sidles, J.L. Garbini, K.J. Bruland, D. Rugar, O. Zuger, S. Hoen, C.S. Yannoni, "Magnetic resonance force microscopy", *Rev. Mod. Phys*. **67**, 249 (1995).

[2] C.L. Degen, M. Poggio, H.J. Mamin, C.T. Rettner, D. Rugar, "Nanoscale magnetic resonance imaging", *Proc. Natl. Acad. Sciences* **106**, 1313 (2009).

[3] W.F. Koehl, B.B. Buckley, F.J. Heremans, G. Calusine, D.D. Awschalom, "Room temperature coherent control of defect spin qubits in silicon carbide", *Nature* **479,** 84 (2011).

[4] D. Riedel, F. Fuchs, H. Kraus, S. Vath, A. Sperlich, V. Dyakonov, A. A. Soltamova, P. G. Baranov, V.A. Ilyin, and G.V.Astakhov, "Resonant Addressing and Manipulation of Silicon Vacancy Qubits in Silicon Carbide", *Phys. Rev. Lett.* **109,** 226402 (2012).

[5] N. Mizuochi, S. Yamasaki, H. Takizawa, N. Morishita, T. Ohshima, H. Itoh, and J. Isoya, "Continuous-wave and pulsed EPR study of the negatively charged silicon vacancy with *S=1/2* and C_{3v} symmetry in *n*-type 4*H*-SiC", *Phys. Rev. B* **66,** 235202 (2002).

[6] R. Kolesov, K. Xia, R. Reuter, R. Stöhr, A. Zappe, J. Meijer, P.R. Hemmer, J. Wrachtrup, "Optical detection of a single rare-earth ion in a crystal", *Nature Comms.* **3**, 1029 (2012).

[7] M. Zhong, M.P. Hedges, R.L. Ahlefeldt, J.G. Bartholomew, S.E. Beavan, S.M. Wittig, J.J. Longdell, M.J. Sellars, "Optically addressable nuclear spins in a solid with a six-hour coherence time", *Nature* **517**, 177 (2015).

[8] A.M. Tyryshkin, S. Tojo, J.J.L. Morton, H. Riemann, N.V. Abrosimov, P. Becker, H-J. Pohl, T. Schenkel, M.L.W. Thewalt, K.M. Itoh, S.A. Lyon, "Electron spin coherence exceeding seconds in high-purity silicon", *Nature Mat.* **11**, 143 (2012).

[9] G.W. Morley, M. Warner, A.M. Stoneham, P.T. Greenland, J. van Tol, C.W.M. Kay, G. Aeppli, "The initialization and manipulation of quantum information stored in silicon by bismuth dopants", *Nature Mat.* **9**, 725 (2010).

[10] V. Acosta, P. Hemmer, "Nitrogen-vacancy centers: Physics and applications", *MRS Bulletin* **38**, 127 (2013).

[11] T. Staudacher, F. Shi, S. Pezzagna, J. Meijer, J. Du, C. A. Meriles, F. Reinhard, J. Wrachtrup, "Nuclear Magnetic Resonance Spectroscopy on a (5-Nanometer)3 Sample Volume," *Science* **339**, 561 (2013).

[12] H.J. Mamin, M. Kim, M.H. Sherwood, C.T. Rettner, K. Ohno, D.D. Awschalom, D. Rugar, "Nanoscale Nuclear Magnetic Resonance with a Nitrogen-Vacancy Spin Sensor," *Science* **339**, 557 (2013).

[13] S.J. DeVience, L.M. Pham, I. Lovchinsky, A.O. Sushkov, N. Bar-Gill, C. Belthangady, F. Casola, M. Corbett, Hu. Zhang, M.D. Lukin, H. Park, A. Yacoby, R.L. Walsworth, "Nanoscale NMR Spectroscopy and Imaging of Multiple Nuclear Species", arxiv:1406.3365.

[14] A.O. Sushkov, I. Lovchinsky, N. Chisholm, R.L. Walsworth, H. Park, M.D. Lukin, "Magnetic Resonance Detection of Individual Proton Spins Using Quantum Reporters", *Phys. Rev. Lett.* **113**, 197601 (2014).

[15] C. Müller, X. Kong, J-M. Cai, K. Melentijevic´, A. Stacey, M. Markham, D. Twitchen, J. Isoya, S. Pezzagna, J. Meijer, J.F. Du, M.B. Plenio, B. Naydenov, L.P. McGuinness, F. Jelezko, "Nuclear magnetic resonance spectroscopy with single spin sensitivity", *Nature Commun.* **5**, 4703 (2014).

[16] D. Pagliero, A. Laraoui, J. Henshaw, C.A. Meriles, "Recursive polarization of nuclear spins in diamond at arbitrary magnetic fields", *Appl. Phys. Lett.* **105**, 242402 (2014).

[17] R.R. Ernst, G. Bodenhausen, A. Wokaum, *Principles of Nuclear Magnetic Resonance in One and Two Dimensions* (Clarendon Press, Oxford, 1987).

[18] D.M. Toyli, C.F. de las Casas, D.J. Christle, V.V. Dobrovitski, D.D. Awschalom, "Fluorescence thermometry enhanced by coherence of single spins in diamond", *Proc. Natl. Acad. Sci. USA* **110**, 8417 (2013).

[19] H.J. Mamin, M.H. Sherwood, M. Kim, C.T. Rettner, K. Ohno, D.D. Awschalom, D. Rugar, "Multipulse Double-Quantum Magnetometry with Near-Surface Nitrogen-Vacancy Centers", *Phys. Rev. Lett.* **113**, 030803 (2014).

[20] U. Haeberlen, *High Resolution NMR in Solids* (Academic Press, New York, 1976).

[21] A. Laraoui, C.A. Meriles, "Approach to dark spin cooling in a diamond nanocrystal", *ACS Nano* **7**, 3403 (2013).

[22] F. Shi, Q. Zhang, P. Wang, H. Sun, J. Wang, X. Rong, M. Chen, C. Ju, F. Reinhard, H. Chen, J. Wrachtrup, J. Wang, J. Du, "Single protein spin resonance spectroscopy under ambient conditions", *Science* **347**, 1135 (2015).

[23] D. Abrams, M.E. Trusheim, D. Englund, M.D. Shattuck, C.A. Meriles, "Dynamic nuclear spin polarization of liquids and gases in contact with nanostructured diamond", *Nano Letters* **14**, 2471 (2014).

[24] P. London, J. Scheuer , J-M Cai, I. Schwarz, A. Retzker, M.B. Plenio, M. Katagiri, T. Teraji, M. Koizumi, J. Isoya, R. Fischer, L.P. McGuinness, B. Naydenov, F. Jelezko, "Detecting and Polarizing Nuclar Spins with Double Resonance on a Single Electron Spin", *Phys. Rev. Lett.* **111**, 067601 (2013).

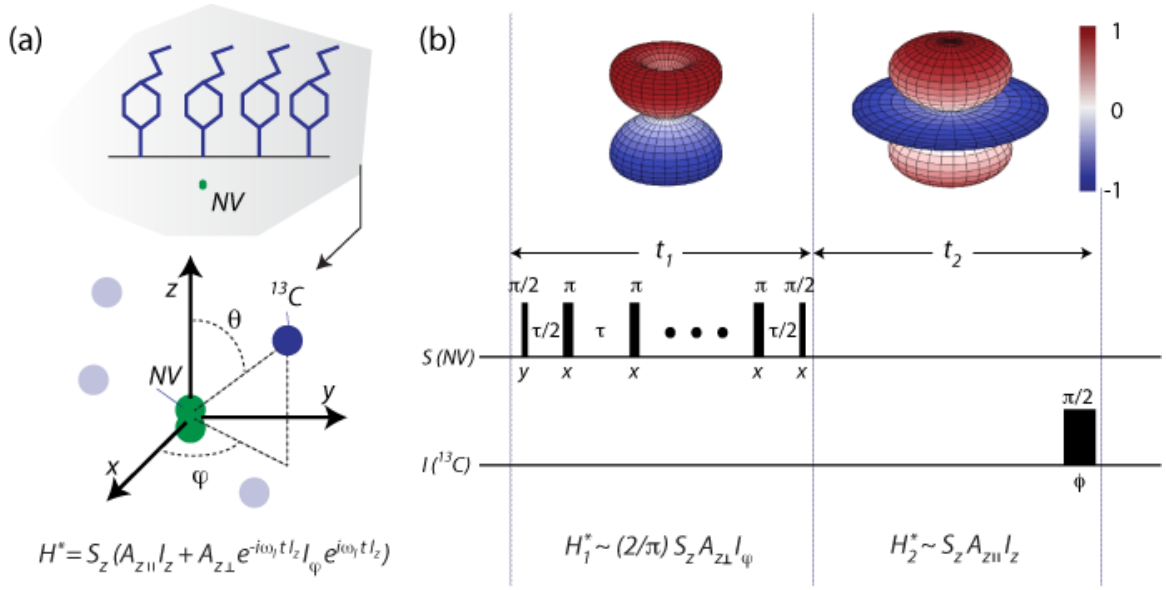

Fig. 1: Spatial encoding via spin polarization transfer. (a) Schematics of an NV center and interacting nuclear spins. One intriguing possibility is the use of shallow NVs to locate spin-labeled nuclei from molecules on the diamond surface. denotes the double-rotating-frame Hamiltonian governing an individual NV-^{13}C pair interacting via a weak hyperfine coupling. (b) Double resonance pulse protocol. A magnetic field B is applied along z, coincident with the NV symmetry axis. The NV is initialized into and all microwave pulses induce transitions between the states. denotes the NV-^{13}C density matrix, here evaluated at different points of the pulse protocol, and , , is the effective time-independent Hamiltonian during each half of the pulse sequence. In each case, the top graph indicates the normalized ^{13}C dipolar coupling as a function of the azimuthal and polar angles (respectively, and in (a)).

Laraoui et al., Fig. 2

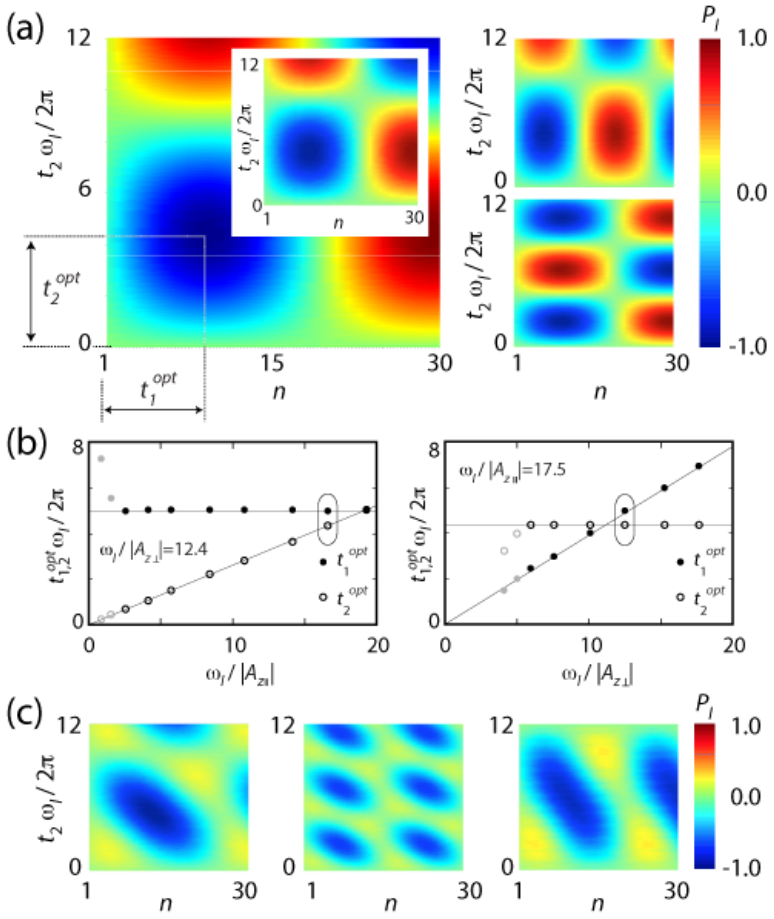

Fig. 2: Pulsed spin polarization transfer to ^{13}C. (a) (Right) Numerically calculated ^{13}C spin polarization after application of the pulse sequence in Fig. 1. The initial NV state is m_S=1, the applied magnetic field is 30 mT, and the hyperfine coupling constants are $A_{z\perp}/2\pi = 25.9$ kHz, $A_{z\parallel}/2\pi = -18.3$ kHz corresponding to spatial coordinates $(r = 0.9\text{ nm},\ \theta = 70.5°,\ \varphi = 0°)$. The insert represents the nuclear polarization as derived from average Hamiltonian theory (Eq. (S15) in Section S2 of the supplementary material). (Left) Numerically calculated ^{13}C spin polarization assuming $A_{z\perp}/2\pi = 39.0$ kHz, $A_{z\parallel}/2\pi = -18.3$ kHz (top panel) and $A_{z\perp}/2\pi = 25.9$ kHz, $A_{z\parallel}/2\pi = -38.0$ kHz (lower panel). (b) Optimum transfer times t_1^{opt} and t_2^{opt} (full and empty circles, respectively) as a function of $\omega_I/A_{z\parallel}$ (right plot, $A_{z\perp}/2\pi = 25.9$ kHz) and $\omega_I/A_{z\perp}$ (left plot, $A_{z\parallel}/2\pi = -18.3$ kHz). The circled pair of dots corresponds to the main case in (a). Lines indicate the relations $t_1^{opt} = \pi^2/(4A_{z\perp})$ and $t_2^{opt} = \pi/(2A_{z\parallel})$ serving as a guide to the eye. (c) Same as in (a) but for mw pulses acting on the NV $m_S = 0 \leftrightarrow m_S = +1$ transition. The ^{13}C angular coordinates are the same but the distance to the NV is 0.7 nm corresponding to $A_{z\perp}/2\pi = 55$ kHz, $A_{z\parallel}/2\pi = -39$ kHz. In (a) through (c) the rf-phase is $\phi = 0$, and the separation between π-pulses is $\tau = \pi/\omega_I$.

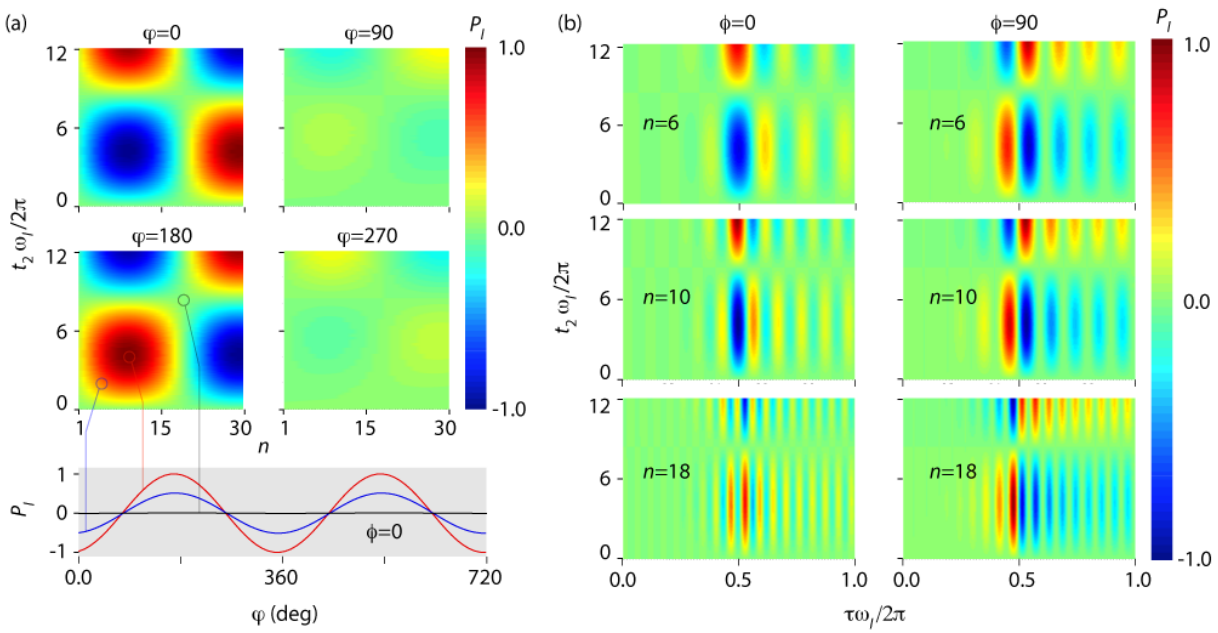

Fig. 3: The role of rf phase and mw timing. (a) Upper panels: Nuclear spin polarization P_I as a function of n, the number of π-pulses, and t_2 for a ^{13}C spin with variable azimuthal coordinate φ. The rf phase is $\phi = 0$. A similar dependence is obtained for a fixed nuclear spin site as one changes the rf phase. Lower panel: P_I as a function of φ for $n = 10$, $\omega_I t_2/2\pi = 4.2$ (red curve), for $n = 6$, $\omega_I t_2/2\pi = 2.1$ (blue curve), and for $n = 19$, $\omega_I t_2/2\pi = 8.2$ (black curve). In all cases the rf phase is $\phi = 0$. (b) Nuclear spin polarization as a function of the normalized inter-pulse separation τ and free evolution interval t_2 for CPMG trains with n π-pulses. Plots on the left (right) column correspond to rf phase $\phi = 0$ ($\phi = 90$). In (a) and (b) the NV interacts with ^{13}C spin located at ($r = 0.9$ nm, $\theta = 70.5°$, $\varphi = 0°$).

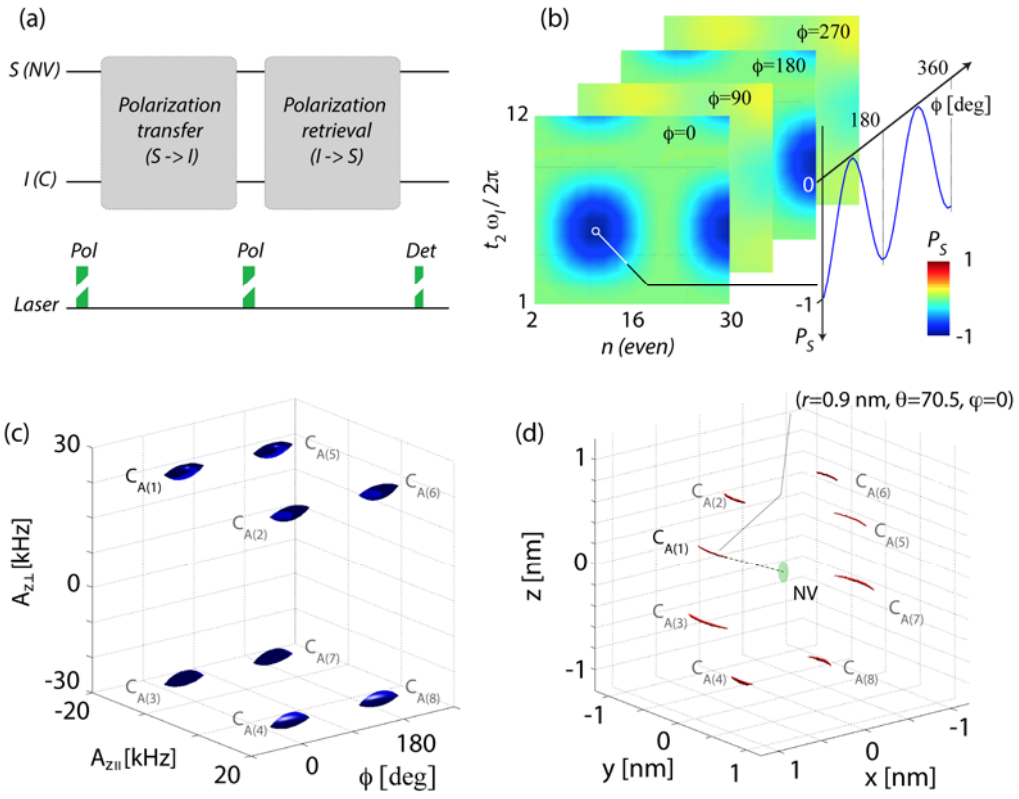

Fig. 4: Determining the nuclear spin position. (a) Schematics of the pulse sequence. Discontinued laser pulses indicate NV polarization into (or detection of) m_S=+1. (b) NV response P_S as a function of the polarization exchange intervals t_1 and t_2 and rf phase ϕ for a single ^{13}C spins with coordinates ($r = 0.9$ nm, $\theta = 70.5°$, $\varphi = 0°$). For clarity, only one maximum is shown but we assume a full data set whose decay is governed by the NV lifetime. (c) Isolevel plot of the 3D spectrum (magnitude mode) upon Fourier transform of the data set in (a) along the time dimensions t_1 and t_2. The corresponding 3D map with the ^{13}C location (right) can be calculated via the transformation $(A_{z\parallel}, A_{z\perp}, \phi) \rightarrow (r, \theta, \varphi)$. Besides the 'real' position (labeled $C_{A(1)}$ in the 3D plots) there are seven 'ghost' images ($C_{A(2)}$… $C_{A(8)}$) arising from a sign ambiguity in each dimension. All surfaces in (c) and (d) correspond to 80% of the NV signal maximum; the NV coherence lifetime is 150 µs.

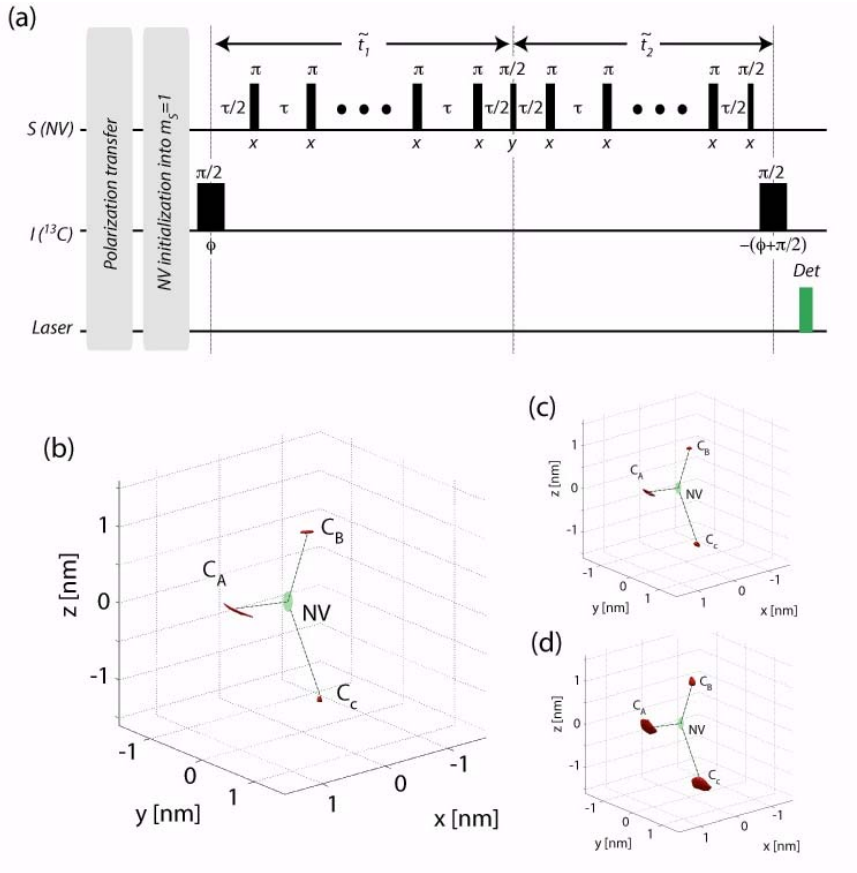

Fig. 5: Imaging a ^{13}C cluster. (a) All ambiguities in the nuclear spin location can be removed with the aid of alternate polarization retrieval protocols. The schematics shows one such protocol where the NV signal is imprinted with the relative sign of the hyperfine coupling constants (see text and Section S2 of the supplementary material). (b) We determine the locations of three ^{13}C spins (denoted as $C_A = (r = 0.90\,\text{nm},\ \theta = 70.5°,\ \varphi = 0°)$, $C_B = (r = 1.03\,\text{nm},\ \theta = 35.3°,$ $\varphi = 60°$, and $C_C = r = 1.03$ nm, $\theta = 144.7°,\ \varphi = 135°$) weakly coupled to an NV (represented by a central green dot). Using three complementary retrieval protocols (including that shown in (a)) we eliminate all ghost images. As in Fig. 4, the red surfaces correspond to isolevel plots of the transformed spectrum at 80% of the NV signal maximum. The NV coherence lifetime is 150 μs. (c-d) Same as in (b) but for NV coherence lifetimes of 75 μs and 38 μs, respectively.